



Dissolution behavior of MgO–pyrochlore composites in acidic solutions

P. Xu ^{a,*}, K. Holliday ^b, K.R. Czerwinski ^b, J.C. Nino ^a

^a Department of Materials Science and Engineering, University of Florida, 100 Rhines Hall, Gainesville, FL 32611, USA

^b Department of Chemistry and Harry Reid Center, University of Nevada, Las Vegas, NV 89154, USA

ARTICLE INFO

Article history:

Received 26 February 2009

Accepted 4 August 2009

ABSTRACT

The dissolution behavior of sintered MgO–pyrochlore ($\text{Nd}_2\text{Zr}_2\text{O}_7$ was chosen for this study) composites in HNO_3 and H_2SO_4 solutions has been studied. The dissolution in 11 M HNO_3 and 7.9 M H_2SO_4 at 60 °C resulted in a selective dissolution of MgO. It was found that initially the fraction of dissolved MgO increases linearly with dissolution time. Magnetic bar stirring enhanced the mass transfer rate and resulted in a higher dissolution rate of MgO compared with the static and ultrasonic dissolution. It also provided mechanical forces to completely disintegrate the undissolved $\text{Nd}_2\text{Zr}_2\text{O}_7$ porous matrix into residual powder. Both MgO and $\text{Nd}_2\text{Zr}_2\text{O}_7$ can be dissolved in boiling concentrated (18 M) H_2SO_4 , and $\text{Nd}_2\text{Zr}_2\text{O}_7$ dissolves incongruently. The dissolution of Mg^{2+} and Nd^{3+} followed first order kinetics, but Zr^{4+} precipitated out due to low solubility in concentrated H_2SO_4 .

© 2009 Elsevier B.V. All rights reserved.

1. Introduction

The kinetics of dissolution of metal oxides in acidic solutions has been extensively studied and the knowledge has been applied in various fields such as metal etching, extraction of ores, removal of deposits from thermal power equipment, and nuclear fuel reprocessing [1–10]. Inert matrix fuel (IMF) is a type of nuclear fuel that utilizes non-fertile materials as a dilute matrix for transmutation of civil and weapon-grade plutonium (Pu) in light water reactors [11–14]. The IMF can be either a once-through type fuel that is subject to direct geological disposal, or a multi-recycling type fuel that is subject to reprocessing. In the latter case, the fissionable materials in spent nuclear fuels should be dissolvable in aqueous solutions so that they can be extracted and separated. The PUREX extraction process developed in the late 1940s and early 1950s in the US was first used to extract Pu and U from a nitric acid solution of dissolved spent fuel [15,16]. A different separation process called UREX + process has recently been studied and developed as a proliferation resistant alternative to the PUREX process [6]. Among those reprocessing techniques, dissolution of spent nuclear fuels in aqueous solution is always the first step. Recently, MgO–pyrochlore ($\text{Nd}_2\text{Zr}_2\text{O}_7$ was chosen in this study) composites were proposed as an inert matrix (IM) candidate material [17]. To assess the possibility of aqueous reprocessing of this IM material, the dissolution behavior of the composites in acids was studied and the results are presented in this paper.

Dissolution of metal oxide in acids involves production and transfer of multiple species, and is a heterogeneous process. The

dissolution reaction can be characterized by whether charge transfer is involved or not. For ionic and covalent oxides, generally speaking, dissolution reaction does not involve charge transfer. Two mechanisms that lead to dissolution of ionic and covalent oxides in aqueous solutions simply are electrophilic attack and nucleophilic attack. The electrophilic attack refers the process that surface oxygen atoms are attacked by positively charged ions from solution, such as hydrogen ion (H^+). The nucleophilic attack occurs on surface metal ions which adsorb negatively charged ions from solution. A typical nucleophile is hydroxyl ion (OH^-). Some other anions are more powerful than OH^- , such as fluoride (F^-), phosphate ion ($(\text{PO}_4)^{3-}$), sulfate ion ($(\text{SO}_4)^{2-}$), and complexation ligands such as EDTA. MgO is a common ionic oxide. The dissolution behavior of MgO in acidic solutions have been extensively studied, and it is known that MgO can be dissolved readily in most acids due to its high ionicity [1,18–26]. On the other hand, most pyrochlore compounds are chemically resistant in general and the dissolution rates are much smaller [27–29]. Pyrochlore $\text{Nd}_2\text{Zr}_2\text{O}_7$ is a Zr contained compound and is a derivative of the fluorite structure. Efforts have been made on digestion of ZrO_2 , a compound which also has a fluorite type structure; it was found that dissolution of ZrO_2 typically requires using hydrofluoric acid (HF) or concentrated sulfuric acid (H_2SO_4) at high temperature or high pressure conditions [30,31]. Microwave digestion has also been studied but corrosive etchant such as HF or concentrated H_2SO_4 is still required [32,33]. Medvedev [7] and his co-workers investigated the dissolution behavior of a cer-cer composite MgO– ZrO_2 in nitric acid at ~55 °C and found that only MgO was able to be dissolved and ZrO_2 was not soluble in HNO_3 . The dissolution behavior of the MgO–pyrochlore composites has not been studied, yet. Therefore, the main objectives of this research work are to study

* Corresponding author. Tel.: +1 352 846 3768; fax: +1 352 846 3355.
E-mail address: pengxu@ufl.edu (P. Xu).

the dissolution behavior of the sintered MgO–pyrochlore composites in acidic solutions, and to search for simple and effective dissolution methods and etchants that are suitable for aqueous reprocessing.

2. Experimental procedure

2.1. Material synthesis

Nd₂Zr₂O₇ pyrochlore was synthesized through sol–gel processing and conventional solid state processing. The precursors used in the sol–gel processing were neodymium nitrate hexahydrate Nd(NO₃)₃ · 6H₂O (Alfa Aesar, 99.9%) and zirconium n-propoxide (Alfa Aesar, 70% w/w in n-propanol). The oxide powders used in the conventional solid state processing were neodymium oxide Nd₂O₃ (Alfa Aesar 99.9%) and zirconium oxide ZrO₂ (Alfa Aesar 99.7%). Magnesium oxide MgO, was calcined from magnesium carbonate, MgCO₃ (Fisher Scientific, 40.0–43.5% MgO) at 900 °C for 2 h. Details of materials synthesis can be found in a previous publication [17]. The synthesized MgO and Nd₂Zr₂O₇ powder was ball milled in ethanol for 24 h. The Nd₂Zr₂O₇ and MgO powders were mixed by ball milling and the volume fraction of MgO varied from 40% to 70%. The mixtures were combined with 2 wt.% of PVA binder (Celvol 103 Polyvinyl Alcohol) and ground with an alumina mortar and pestle until the powder could be sieved through a 212 μm mesh. The sieved powder was then dried in an oven at 120 °C for 5 min. The sieved powder was loaded into a punch and die-set and pressed into a cylindrical green pellet with a diameter varying from 7 mm to 13 mm using Carver cold uniaxial press at 200 MPa, and then sintered in air at various temperatures from 1400 °C to 1650 °C for 4 h. The diameter of the sintered pellets varies from 5 mm to 11 mm, and the thickness of the samples varies from 1 mm to 2 mm. The overall density of the sintered pellets was obtained geometrically. The density of obtained samples varied from 84% to 98% depending on sintering temperature.

2.2. Dissolution test setup

Three dissolution methods were applied, including static dissolution, dynamic dissolution and ultrasonic dissolution. The static dissolution tests were carried out in a 250 mL beaker filled with 100 mL aqueous solution. Samples were immersed in the solution with no agitation. The dynamic dissolution tests were performed in 100 mL solution in a flask connected with a water cooled condenser. To provide uniform heat and constant mechanical agitation, the flask and thermometer were immersed in a water bath heated on a hot plate and agitated by a magnetic bar in the solution. The magnetic bar was usually stirring at a constant rate of 350 rpm. In the ultrasonic dissolution tests, an ultrasonic bath with a capacity of 2.8 L and 40 kHz transducer (Fisher Scientific Mechanical Ultrasonic Cleaners, Model FS20H) was used, and the tests were carried out by positioning a 250 mL flask in the central top zone of the sonication bath at 60 °C. The power delivered in each sonicated run was obtained calorimetrically by determining the temperature rise over the first 5 min of input using the following equation [34,35]:

$$\text{Power (W)} = \frac{dT}{dt} \cdot m \cdot s, \quad (1)$$

where T is the temperature (K), t is time (s), m is mass of solution (g) and s is the specific heat of the solution (J/g K).

Solution samples of 0.3 mL were drawn from the beaker at certain time intervals using a micron pipette with an error in the range of 10%, and these samples are diluted to 12 mL solution by

adding distilled water and stored in a 15 mL low alkali glass vial. The ion concentrations in sample solutions were measured using inductively coupled plasma atomic emission spectroscopy (ICP-AES, Perkin–Elmer Plasma 3200). The dissolved ion concentrations were calculated by multiplying the measured ion concentration, the dilution factor and the volume of solvent.

In an attempt to dissolve pyrochlore Nd₂Zr₂O₇, the dissolution tests were also conducted in the boiling concentrated (18 M) H₂SO₄ (Alfa Aesar, reagent grade) in the Department of Chemistry and Harry Reid Center at the University of Nevada, Las Vegas. Samples were placed in concentrated H₂SO₄ (200 mL) in a round bottom flask equipped with reflux condensers and heated to boiling using a heating mantle. Samples were taken periodically using glass Pasteur pipettes. Once cooled 0.5 mL of solution was pipetted from the samples using a quantitative pipette, and the ion concentrations were measured using a Spectro Ciros ICP-AES.

2.3. Structural characterization

The microstructure and crystal structure of the composites were characterized using scanning electron microscopy (SEM) and X-ray diffraction (XRD). All SEM samples were sputtered with a carbon film with thickness of about 20 nm and were analyzed with field-emission SEM (JEOL 6335F). The XRD profile of the samples was obtained using an X-ray diffractometer (XRD-Philips APD 3720). The particle size and size distribution of dissolution residue were characterized using laser light scattering (Beckman Coulter LS 13320). The samples collected for particle size measurement were suspended in deionized water and placed in an ultrasonic bath for 30 s before analysis.

3. Results and discussion

3.1. Dissolution of the MgO–Nd₂Zr₂O₇ composites in HNO₃

Since HNO₃ is widely used in the current reprocessing techniques, the dissolution behavior of MgO–Nd₂Zr₂O₇ composites in HNO₃ was the initial focus of this study. High molarity of HNO₃ (11 M) (Ricca Chemical, 70% (v/v) aqueous solution) was selected for all tests to achieve high activity and dissolution rate. The fraction of consumed H⁺ ions during dissolution is on the order of 10^{−3}, suggesting that the dissolution reaction has a minimum effect on the pH. The molarity of dissolved Mg²⁺ ions was always less than 0.1 mol/L, which is at least one order of magnitude lower than the saturation concentration (the solubility of Mg(NO₃)₂ is calculated to be 6.2 mol/L at 60 °C [36]), indicating that the dissolution reaction has not reached equilibrium.

Table 1 summarizes sample information, dissolution conditions and products for each experiment conducted in this study.

3.1.1. Dynamic dissolution and dissolution rate of MgO

Fig. 1 shows the results of test #1 listed in Table 1. The test was conducted at 60 °C with magnetic bar stirring. The composite consists of 70 vol.% MgO with a density of 96%. It was found that only Mg²⁺ ions were leached out from the composite, and that no Nd³⁺ or Zr⁴⁺ ions were detected in solution. The instrumental errors were taken into account for measuring sample weight, geometry, and solvent volume. Final errors were calculated and expressed as error bars in the figure.

For a heterogeneous reaction such as the dissolution of metal oxides in aqueous solutions, the rate of reaction depends on the intrinsic mass transfer coefficient k_{s1} , the surface area S , and the driving force of concentration difference ($C_{eq} - C$), as shown below:

$$R = k_{s1} \cdot S \cdot (C_{eq} - C), \quad (2)$$

Table 1

Sample and acid information, dissolution condition and products.

Test#	Sample composition (vol.% of MgO)	Sample mass (g)	Sample diameter (ϕ) and thickness (t) (mm)	Sample density (%TD)	Solvent, method, temperature and exposure time	Dissolution product (s: solid, aq: aqueous)
1	70	0.4891	ϕ 10.66, t 1.30	95.5	11 M, HNO ₃ , magnetic bar stir, 60 °C and 25 h	Nd ₂ Zr ₂ O ₇ (s), Mg ²⁺ (aq)
2	70	0.4885	ϕ 10.60, t 1.27	98.7	11 M, HNO ₃ , magnetic bar stir, 20 °C and 476 h	Nd ₂ Zr ₂ O ₇ (s), Mg ²⁺ (aq)
3	70	0.0866	ϕ 5.32, t 0.96	92.4	11 M, HNO ₃ , magnetic bar stir, 60 °C and 23 h	Nd ₂ Zr ₂ O ₇ (s), Mg ²⁺ (aq)
4	70	0.2195	ϕ 7.85, t 1.17	88.2	11 M, HNO ₃ , magnetic bar stirring, 60 °C and 125 h	Nd ₂ Zr ₂ O ₇ (s), Mg ²⁺ (aq)
5	60	0.2002	ϕ 9.51, t 0.68	88.3	11 M, HNO ₃ , magnetic bar stirring, 60 °C and 3 h	Nd ₂ Zr ₂ O ₇ (s), Mg ²⁺ (aq)
6	40	0.1111	ϕ 5.79, t 0.91	88.2	11 M, HNO ₃ , magnetic bar stirring, 60 °C and 10 h	Nd ₂ Zr ₂ O ₇ (s), Mg ²⁺ (aq)
7	70	0.4981	ϕ 10.58, t 1.30	98.7	11 M, HNO ₃ , static, 60 °C and 70 h	Nd ₂ Zr ₂ O ₇ (s), Mg ²⁺ (aq)
8	70	0.4885	ϕ 10.66, t 1.27	97.6	11 M, HNO ₃ , ultrasound, 60 °C and 52 h	Nd ₂ Zr ₂ O ₇ (s), Mg ²⁺ (aq)
9	70	0.4885	ϕ 10.60, t 1.27	98.7	7.9 M, H ₂ SO ₄ , magnetic bar stirring, 60 °C and 55 h	Nd ₂ Zr ₂ O ₇ (s), Mg ²⁺ (aq)
10	50	0.401	ϕ 7.92, t 1.95	84.0	18 M, H ₂ SO ₄ , magnetic bar stirring, 338 °C and 173 h	Mg ²⁺ (aq), Nd ³⁺ (aq), Zr ⁴⁺ (aq), unknown solid phase

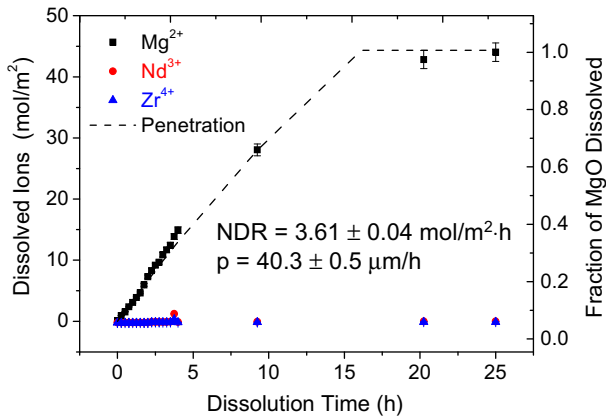


Fig. 1. Dynamic dissolution of the composite with 70 vol.% of MgO in 11 M HNO₃ at 60 °C.

where C_t is the ion concentration at time t . To compare the dissolution rates at different dissolution conditions, examining the initial rate where the solutions are far from equilibrium is a common approach [37,38]. The dissolution rate is typically normalized by the surface area. Since only MgO can be dissolved, the dissolution rate of MgO was normalized by its geometric area. The geometric area of MgO was calculated by multiplying the MgO volume fraction and the total geometric area of the composite. The calculation is based on the conclusion that the area fraction of one phase in a random 2D section plane in a composite equals to its overall volume fraction [39]. In Fig. 1, the y-axis on the left shows the geometric area normalized ions in solution, which is converted into dissolved fraction shown on the right y-axis. As the figure shows, the dissolution of MgO was completed after 25 h. A linear relationship was found between the number of dissolved Mg²⁺ ions and the dissolution time at the beginning of dissolution, so the normalized dissolution rate (NDR) of MgO can be described by:

$$\text{NDR} = \frac{V}{A_{\text{MgO}}} \cdot \frac{dC}{dt} \quad (3)$$

where V is equal to the volume of solvent, A_{MgO} is the initial geometric area of MgO, and dC/dt is the change of the concentration as a function of time, which can be obtained by fitting the data using linear regression. The calculated NDR for this test is 3.61 mol/m² h.

The temperature effect on the NDR of MgO was evaluated by conducting another dynamic test at room temperature around 20 °C (test #2 in Table 1) and comparing the results with the one obtained at 60 °C. It is found that the NDR of MgO increases by a

factor of 36 as the temperature increases from 20 °C to 60 °C, indicating the temperature has great effect on the NDR of MgO.

The dissolution of spherical particles in aqueous solutions can be associated with the well-known shrinking core models, and the rate controlling mechanism can be classified into liquid film diffusion, surface reaction and product layer diffusion [40]. However, the composite has a finite cylindrical shape and the dissolution is selective, which significantly complicates the model. Since the pellet has a relatively large aspect ratio greater than 8 with diameter to thickness, the flat plate model can be used as an approximate for the initial dissolution of MgO because the initial change on the radial direction is not significant. In the case of flat plate, the three mechanisms can be expressed as follows:

$$x = k_f t, \quad \text{for film diffusion control} \quad (4)$$

$$x^2 = k_D t, \quad \text{for product layer diffusion control} \quad (5)$$

$$x = k_S t, \quad \text{for surface reaction control} \quad (6)$$

where x is dissolved fraction at time t and k_f , k_D , k_S are apparent rate constants. For the dynamic dissolution, the film diffusion can be eliminated due to strong stirring [32]. Therefore, the obtained linear relationship between the dissolved fraction and dissolution time indicates that dissolution of MgO is a surface reaction controlled process at this reaction condition.

To obtain a better model for describing the dissolution behavior of MgO, the flat plate model was modified, and a new model was proposed by taking into account the shrinkage on the radial direction. By assuming that nitric acid penetrates at a constant rate from the outer surface of the composite to the interior and is able to dissolve MgO completely at the penetration depth, the penetration rate p (or the rate of displacement of the interface), can then be calculated in this formula [38]:

$$p = \frac{M}{\rho} R, \quad (7)$$

where p is the penetration rate, M is the molecular mass of MgO, ρ is the density of MgO and R is the NDR of MgO. For the same test conducted at 60 °C, the penetration rate was calculated to be 40.3 µm/h. The dissolution curve was then calculated based on this model and is plotted as a dashed line shown in Fig. 1.

3.1.2. Effect of sample porosity and MgO volume fraction on the NDR of MgO

Fig. 2a compares the initial dissolution for the composites with densities varying from 88.2% to 95.5% (tests #1, #3 and #4 in Table 1), and it was found that, as expected, the NDR of MgO increases with sample porosity. The surface area of MgO increases due to the presence of open porosity, and the closed porosity may become open porosity when the adjacent MgO grains are dissolved. The

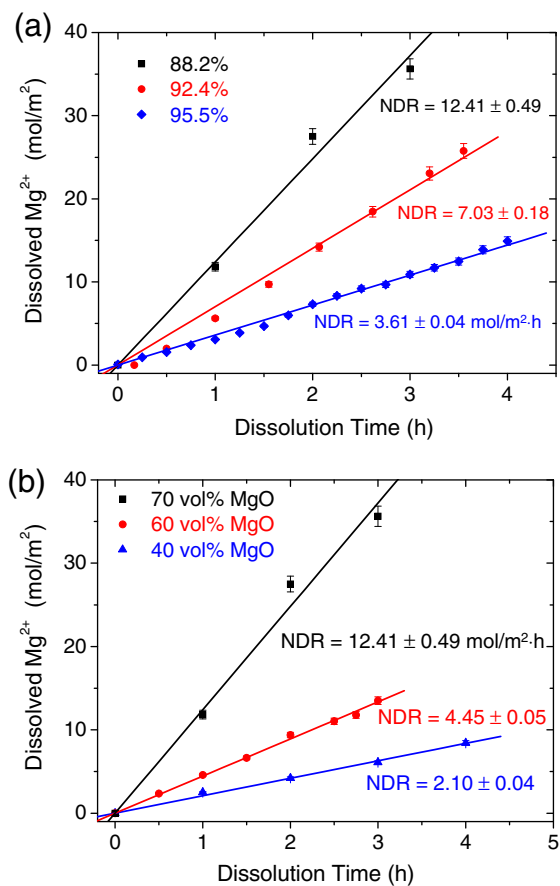


Fig. 2. (a) Effect of sample porosity on NDR of MgO, and (b) effect of MgO volume fraction on NDR of MgO.

pores also provide additional transport channels for the migration of protons and Mg^{2+} ions, so the penetration rate is expected to be increased with porosity.

Fig. 2b compares the initial dissolution curves for the composites with the same density but different MgO volume fraction from 40% to 70% (tests #4, #5 and #6 in Table 1), and it was found that the NDR of MgO increased with the volume fraction of MgO. For a surface reaction controlled process, the dissolution rate is expected to be proportional to the surface area. The geometric area is just the initial surface area, but the true surface area of MgO during dissolution is unknown. It is anticipated that the dissolution reaction proceeds along connected MgO grains. So the contiguity of MgO, which is defined as the fraction of the interface area of MgO that is shared by MgO, is an important determining factor for the surface area of MgO during dissolution [39]. The contiguity of MgO in the composites can be quantified using stereology described in Underwood's book [39], and was found to increase from 0.14 to 0.42 as the volume fraction of MgO increases from 40% to 70% [41]. Therefore, higher contiguity of MgO results in a larger surface area of MgO during dissolution, and correspondingly a higher NDR of MgO.

3.1.3. Characterization of the composites before and after dissolution

The microstructural evolution of the composites tested with magnetic bar stirring was recorded and shown in Fig. 3a–c. Fig. 3a shows microstructure of a sintered composite with 60 vol.% of MgO. The dark grains are MgO and the light grains are $Nd_2Zr_2O_7$. Fig. 3b shows a porous matrix which developed during dissolution. The developed porosity is a result of dissolution of MgO grains, and the interconnected pores serve as transport chan-

nels for HNO_3 to continue digesting the MgO grains inside the matrix. Further magnetic bar stirring resulted in a complete disintegration of the porous matrix due to the constant mechanical agitation. Fig. 3c shows the morphology of the dissolution residue collected at the end of the test, which consists of single grains and grain clusters. The large grain clusters are shown as an inset at the upper right corner. The particle size and size distribution of the residual powder are shown in Fig. 3d. The dissolution residue has a broad size distribution primarily ranging from 1 to 100 μm , and the main peak between 1 and 10 μm corresponds to the size of single grains and small grain clusters. The few minor peaks between 10 and 100 μm indicate that large grain clusters with size above 10 μm are also present in the residue. The results are consistent with the SEM observation in general. Even though HNO_3 alone cannot completely dissolve the composite, disintegration of the undissolved porous matrix is a benefit for dissolution because the surface area of dissolvable phases is expected to increase, which leads to a higher dissolution rate and dissolved fraction.

Fig. 4 shows the XRD profiles for the surfaces of the composite and the porous matrix, and the dissolution residue. By comparing these XRD profiles, it is concluded that the pyrochlore $Nd_2Zr_2O_7$ remained intact during the whole dissolution, and all MgO has been dissolved. The results confirm a selective dissolution of MgO, and there was no phase transformation for pyrochlore $Nd_2Zr_2O_7$ after exposure to 11 M HNO_3 at 60 °C. Since PuO_2 can be dissolved in HNO_3 , it is envisioned that the fissionable materials can be dissolved in a similar way to the dissolution of MgO in HNO_3 as described here. Nevertheless, dissolution tests for Pu or U (as a surrogate for Pu) containing composites should be conducted to further investigate the dissolution behavior of the fissionable materials in this type of IMF.

3.1.4. Static and ultrasonic dissolution

The composites tested here were made from the same batch as those tested in the dynamic dissolution. Fig. 5a shows the results of the static dissolution test (test #7 in Table 1) conducted at 60 °C in 11 M HNO_3 . It was found that only MgO can be dissolved, and the dissolution behavior was similar to the dynamic dissolution. Without agitation, the porous pyrochlore matrix remained intact despite the dissolution of the MgO phase. The NDR of MgO was calculated to be 1.50 mol/m²·h, which is less than half of the NDR obtained from the dynamic dissolution, suggesting the mass transfer rate is lower in the static dissolution, and the dissolution process is limited by film diffusion. The calculated penetration rate was 16.0 $\mu m/h$. The dissolution of MgO was not completed at the end of test, and the dissolved fraction reached about 90% and then leveled off. This could be a result of isolated MgO grains that have minimum connectivity to other MgO grains. Dissolution of these MgO grains is limited by diffusion of reactants and products through $Nd_2Zr_2O_7$ grain boundaries, which is a much slower process compared with the dissolution reaction. By contrast, magnetic bar stirring provides additional mechanical force to disintegrate the porous matrix and break the clusters apart, resulting in a completed dissolution of MgO.

It has been found that ultrasound can accelerate dissolution of metal oxides in aqueous solutions and trigger reactions that do not occur at normal conditions [42,43]. Studies show there are two main effects: one is mechanical effect that can increase mass transfer rate, surface area, and driving force; the other one is chemical effect that initiate reactions caused by formed reactive free radicals [34,44,45]. The preliminary ultrasonic dissolution test was an attempt to dissolve $Nd_2Zr_2O_7$ and further increase NDR of MgO in HNO_3 . The ultrasonic power was measured and the value was 10.3 ± 1.0 W/s. The ultrasound was applied for the first 8 h and then turned off, but the dissolution test continued at a static condition. Fig. 5b shows the results of the ultrasonic dissolution

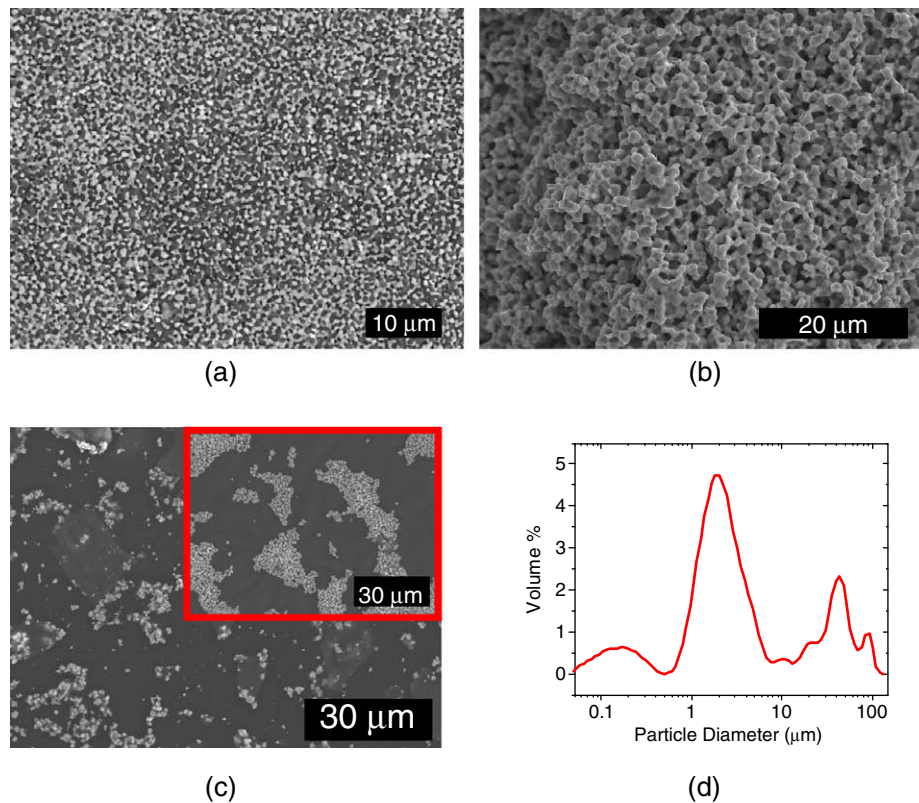


Fig. 3. (a) Microstructure of the composite with 60 vol.% MgO, (b) microstructure of the porous matrix developed during dissolution, (c) morphology of the dissolution residue, and (d) particle size and size distribution of the dissolution residue.

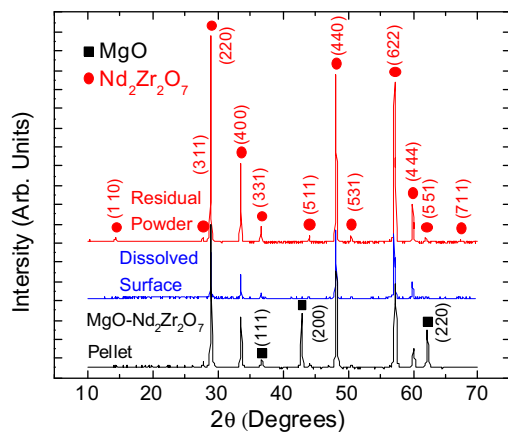


Fig. 4. The XRD profile of the sintered composite, surface of the porous matrix, and the residual powder collected from the flask after dissolution test.

conducted at 60 °C in 11 M HNO₃ (test #8 in Table 1). The obtained NDR of MgO was 1.8 mol/m² h, which is comparable to the static dissolution but much lower than the dynamic dissolution. Nd₂Zr₂O₇ did not dissolve, indicating that ultrasound has no chemical effect on dissolving Nd₂Zr₂O₇ at this reaction condition. The inefficiency of ultrasonic dissolution of MgO was probably due to the large sample size compared with cavitation bubbles. The microstreaming effect is efficient when the size of reactant is comparable to the cavitation bubbles, which are typically in the micron range. Asymmetric implosion of cavitation bubbles on a large surface produces microjets that erode the surface and create active sites, which could also enhance the dissolution rate. Nevertheless, MgO undergoes dramatic surface reconstruction immediately

when exposed to aqueous solutions [46], and the active sites may be already saturated before ultrasound is applied. It is worth noting that the ultrasonic effects depend on the ambient conditions of the reaction system [34]. More reaction conditions should be tested to fully evaluate the ultrasonic effects on dissolution of the composites in HNO₃.

3.2. Dissolution the MgO–Nd₂Zr₂O₇ composites in H₂SO₄

The dissolution of MgO–Nd₂Zr₂O₇ composite in H₂SO₄ (Fisher Chemical, certified ACS plus 95.0–98.0%) was first conducted in 7.9 M H₂SO₄ at 60 °C with magnetic bar stirring (test #9 in Table 1) and the results are plotted in Fig. 6a. The results show similar dissolution behavior and comparable NDR of MgO as to the dynamic dissolution in HNO₃.

In an attempt to dissolve pyrochlore Nd₂Zr₂O₇, the dissolution tests were carried out in boiling concentrated H₂SO₄ (test #10 in Table 1) and the results are plotted in Fig. 6b. The y-axis shows the concentration of the three ions in solution. The obtained results indicate that both MgO and Nd₂Zr₂O₇ can be dissolved in boiling concentrated H₂SO₄. The ability to dissolve Nd₂Zr₂O₇ can be attributed to the presence of strong nucleophile (SO₄)^{2−} in concentrated H₂SO₄. The results indicate that the nucleophilic attack by (SO₄)^{2−} on the cation sites in pyrochlore Nd₂Zr₂O₇ is effective and also efficient at the boiling point of H₂SO₄. It worth noting that dissolution of MgO–Nd₂Zr₂O₇ composites in concentrated H₂SO₄ at room temperature did not lead to a noticeable dissolution of Nd₂Zr₂O₇, which was probably hindered by kinetics factors. Therefore, the concentration of H₂SO₄ and reaction temperature both play important roles in dissolving Nd₂Zr₂O₇. However, due to limited solubility of Nd³⁺ and Mg²⁺ in concentrated H₂SO₄, the dissolution reached equilibrium and neither of them was completely dissolved. The fraction of dissolved Mg²⁺, Nd³⁺ and Zr⁴⁺ were

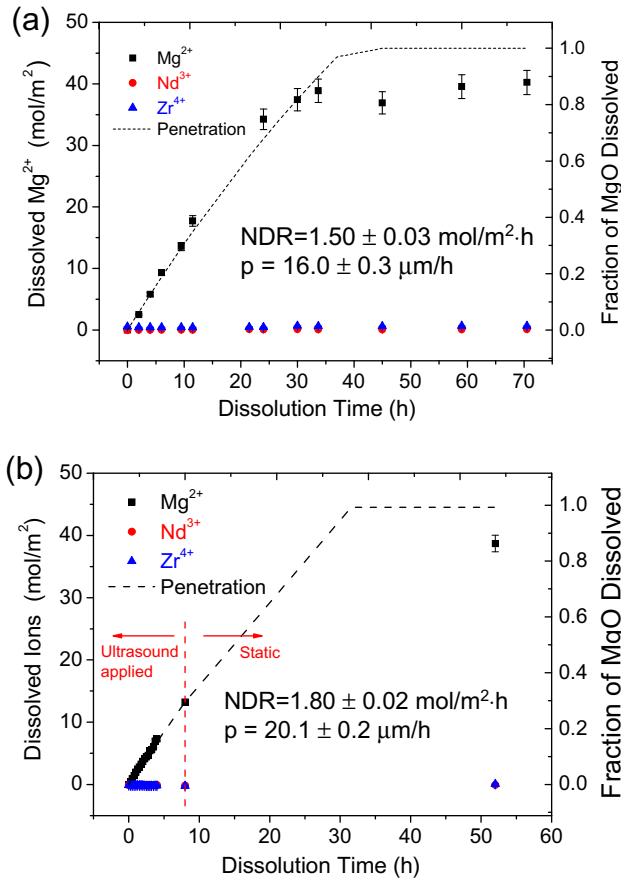


Fig. 5. (a) Static dissolution test and (b) ultrasonic dissolution test in 11 M HNO₃ at 60 °C.

calculated to be 72.9%, 91.8% and 19.3%, respectively, for a 0.4 g composite with 50 vol.% of MgO in 200 mL concentrated H₂SO₄ at its boiling temperature around 338 °C. The dissolution of Mg²⁺ and Nd³⁺ follows first order kinetics and the data points were fitted using first order equation as below:

$$C = C_{eq}(1 - \exp(-kt)), \quad (8)$$

where C is the concentration of ions in solution, t is dissolution time, C_{eq} is the equilibrium concentration, and k is the reaction constant indicating how fast the reaction reaches equilibrium. The reaction constant k and equilibrium constant C_{eq} were obtained from the fit at the boiling point of H₂SO₄ and are shown in the figure. The reaction constant for Nd³⁺ and Mg²⁺ are calculated to be $0.0220 \pm 0.0039 \text{ h}^{-1}$ and $0.0259 \pm 0.0014 \text{ h}^{-1}$, and the equilibrium concentrations of Nd³⁺ and Mg²⁺ in solution are determined to be $0.0041 \pm 0.0003 \text{ mol/L}$ and $0.0133 \pm 0.0003 \text{ mol/L}$. It was observed that the dissolution rate of Nd³⁺ was nearly twice as that of Zr⁴⁺ at the first 20 h, suggesting that Nd₂Zr₂O₇ dissolved non-stoichiometrically in boiling concentrated H₂SO₄ and it was incongruent dissolution. Moreover, dissolution of Zr did not follow the same kinetics. The dissolved Zr was first suspended as colloids in solution through the dissolution of Nd³⁺ from the pyrochlore. As the colloids polymerize they crash out of solution leaving an insoluble compound at the bottom of the flask. This is due to the low solubility of the Zr in concentrated H₂SO₄. By constantly removing dissolution products from the solution, the dissolution reaction can be maintained until desired dissolution fraction is achieved. Therefore, it is possible to dissolve the whole composite in boiling concentrated H₂SO₄, thus eliminating the undesirable use of hydrofluoric acid (HF). Nevertheless, additional steps are required to transfer the dis-

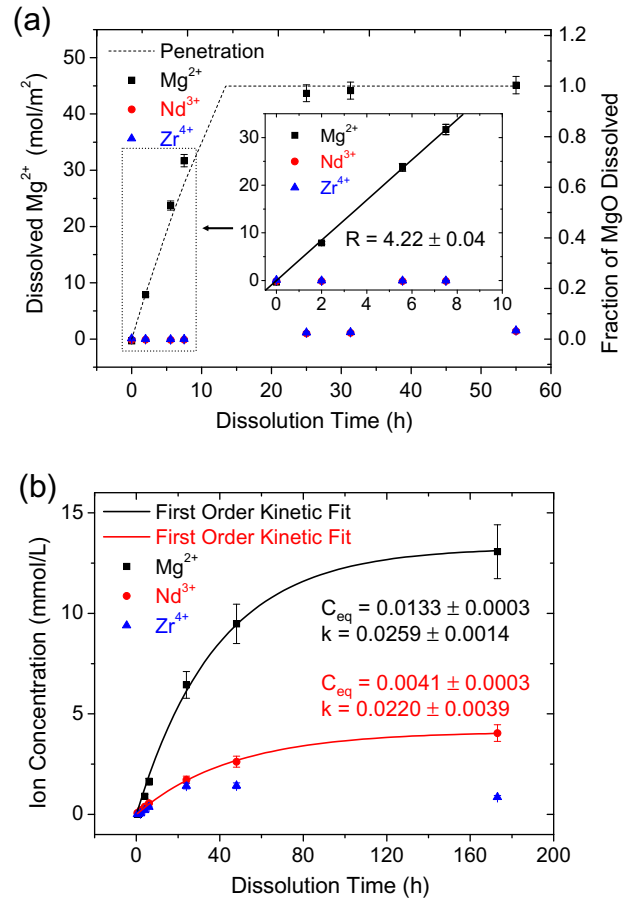


Fig. 6. (a) Dissolution of the composite with 70 vol.% of MgO in 7.9 M H₂SO₄ at 60 °C, and (b) dissolution of the composite with 50 vol.% of MgO in the boiling concentrated H₂SO₄.

solved species including fissile and non-fissile materials from H₂SO₄ to HNO₃, which may increase the complexity and cost of the process.

4. Conclusions

The dissolution behavior of the MgO–Nd₂Zr₂O₇ composites was studied in HNO₃ and H₂SO₄ at different conditions. It is shown that MgO can be dissolved in 11 M HNO₃ and 7.9 M H₂SO₄ at 60 °C, but Nd₂Zr₂O₇ is insoluble. The NDR of MgO depends on the MgO volume fraction, sample porosity, dissolution temperature, and agitation methods. Magnetic bar stirring is an efficient agitation method to accelerate dissolution process and disintegrate the undissolved Nd₂Zr₂O₇ porous matrix into residual powder. Both MgO and pyrochlore Nd₂Zr₂O₇ can be dissolved in boiling concentrated H₂SO₄, but the solubility of Mg²⁺, Nd³⁺ and Zr⁴⁺ are limited compared within aqueous solutions. The dissolution of Mg²⁺ and Nd³⁺ followed first order kinetics, but Zr⁴⁺ precipitated out due to low solubility in concentrated H₂SO₄. By constantly removing dissolution product, it is possible to dissolve the whole composite in boiling concentrated H₂SO₄. Dissolution tests for Pu or U (as a surrogate for Pu) containing IMFs should be performed and evaluated to fully assess the feasibility of aqueous reprocessing of this type of IM material.

Acknowledgements

The authors would like to acknowledge the technical assistance from the Major Analytical Instrumentation Center (MAIC) and

Particle Engineering Research Center (PERC), Department of Materials Science and Engineering, University of Florida. This work is funded by the US Department of Energy through the Nuclear Energy Research Initiative (NERI) Program (DE-FC07-05ID14647).

References

- [1] Dd. Macdonal, D. Owen, *Can. J. Chem.* 49 (1971) 3375.
- [2] I.G. Gorichev, N.A. Kipriyanov, S.K. Vainman, N.P. Shevelev, *J. Appl. Chem.-USSR* 54 (1981) 43.
- [3] I.G. Gorichev, N.A. Kipriyanov, *Usp Khim+* 53 (1984) 1790.
- [4] V.V. Batrakov, I.G. Gorichev, N.A. Kipriyanov, *Russ. J. Electrochem.* 30 (1994) 399.
- [5] H. Mineo, H. Isogai, Y. Morita, G. Uchiyama, *J. Nucl. Sci. Technol.* 41 (2004) 126.
- [6] A.J. Bakel, D.L. Bowers, K.J. Quigley, M.C. Regalbuto, J.A. Stillman, G.F. Vandegrift, *Acs. Sym. Ser.* 933 (2006) 71.
- [7] P.G. Medvedev, M.J. Lambregts, M.K. Meyer, *J. Nucl. Mater.* 349 (2006) 167.
- [8] G.P. Nikitina, Y.E. Ivanov, A.A. Listopadov, L.B. Shpunt, *Radiochemistry* 39 (1997) 12.
- [9] J.M. Cleveland, *J. Inorg. Nucl. Chem.* 26 (1964) 1470.
- [10] B. Tuck, *J. Mater. Sci.* 10 (1975) 321.
- [11] C. Degueldre, T. Yamashita, *J. Nucl. Mater.* 319 (2003) 1.
- [12] R. Chawla, R.J.M. Konings, *Prog. Nucl. Energ.* 38 (2001) 455.
- [13] H. Matzke, V.V. Rondinella, T. Wiss, *J. Nucl. Mater.* 274 (1999) 47.
- [14] C. Degueldre, J.M. Paratte, *J. Nucl. Mater.* 274 (1999) 1.
- [15] D.D. Sood, S.K. Patil, *J. Radioanal. Nucl. Ch. Ar.* 203 (1996) 547.
- [16] D.O. Campbell, W.D. Burch, *J. Radioanal. Nucl. Ch. Ar.* 142 (1990) 303.
- [17] S.J. Yates, P. Xu, J. Wang, J.S. Tulenko, J.C. Nino, *J. Nucl. Mater.* 362 (2007) 336.
- [18] O. Fruhwirth, G.W. Herzog, I. Hollerer, A. Rachetti, *Surf. Technol.* 24 (1985) 301.
- [19] K. Sangwal, S.K. Arora, *J. Mater. Sci.* 13 (1978) 1977.
- [20] P. Raschman, A. Fedorockova, *Chem. Eng. Sci.* 63 (2008) 576.
- [21] P. Raschman, A. Fedorockova, *Chem. Eng. J.* 117 (2006) 205.
- [22] K. Sangwal, T.C. Patel, M.D. Kotak, *J. Mater. Sci.* 14 (1979) 1869.
- [23] K. Sangwal, *J. Mater. Sci.* 17 (1982) 3598.
- [24] K. Sangwal, *J. Mater. Sci.* 15 (1980) 237.
- [25] K. Sangwal, J.N. Sutaria, *J. Mater. Sci.* 11 (1976) 2271.
- [26] K. Sangwal, K.R. Rao, *J. Mater. Sci.* 15 (1980) 2673.
- [27] H.F. Xu, Y.F. Wang, P.H. Zhao, W.L. Bourcier, R. Van Konynenburg, H.F. Shaw, *Environ. Sci. Technol.* 38 (2004) 1480.
- [28] B.D. Begg, N.J. Hess, W.J. Weber, R. Devanathan, J.P. Icenhower, S. Thevuthasan, B.P. McGrail, *J. Nucl. Mater.* 288 (2001) 208.
- [29] S.K. Roberts, W.L. Bourcier, H.F. Shaw, *Radiochim. Acta* 88 (2000) 539.
- [30] D. Merten, J.A.C. Broekaert, R. Brandt, N. Jakubowski, *J. Anal. Atom. Spectrom.* 14 (1999) 1093.
- [31] B.J. Newby, Separation of Uranium from Uranium Dioxide – Zirconium Dioxide Mixtures, 1967, US Patent #3341304.
- [32] M.T. Larrea, I. GomezPinilla, J.C. Farinas, *J. Anal. Atom. Spectrom.* 12 (1997) 1323.
- [33] X.G. Ma, Y.B. Li, *Anal. Chim. Acta* 579 (2006) 47.
- [34] L.H. Thompson, L.K. Doraiswamy, *Ind. Eng. Chem. Res.* 38 (1999) 1215.
- [35] J.P. Lorimer, T.J. Mason, K. Fiddy, *Ultrasonics* 29 (1991) 338.
- [36] O. Sohnel, P. Novotny, *Densities of Aqueous Solutions of Inorganic Substances*, Elsevier, Amsterdam, 1985.
- [37] M.I. Martinez, W.B. White, *J. Cave Karst Studies* 61 (1999) 7.
- [38] M.A. Blesa, P.J. Morando, A.E. Regazzoni, *Chemical Dissolution of Metal Oxides*, CRC Press, Boca Raton, 1994.
- [39] E.E. Underwood, *Quantitative Stereology*, Addison-Wesley, Reading, 1970.
- [40] O. Levenspiel, *Chemical Reaction Engineering*, Wiley, New York, 1999.
- [41] P. Xu, Evaluation of In-service Materials Engineering Parameters for Potential Inert Matrix Materials, Dissertation, University of Florida, 2009.
- [42] P. Moisy, S.I. Nikitenko, L. Venault, C. Madic, *Radiochim. Acta* 75 (1996) 219.
- [43] K.S. Suslick, *Ultrasound: Its Chemical, Physical, and Biological Effects*, VCH Publishers, New York, 1988.
- [44] K.S. Suslick, Y. Didenko, M.M. Fang, T. Hyeon, K.J. Kolbeck, W.B. McNamara, M.M. Mdeleleni, M. Wong, *Philos. T. Roy. Soc. A* 357 (1999) 335.
- [45] K.S. Suslick, G.J. Price, *Annu. Rev. Mater. Sci.* 29 (1999) 295.
- [46] R.S.C. Smart, J. Nowotny, *Ceramic Interfaces – Properties and Applications*, IOM Communications, London, 1998.